Theor Chem Acc (2011) 130:1031–1038
DOI 10.1007/s00214-011-1012-y

REGULAR ARTICLE

Density functional theory study on quasi-three-dimensional oxidized platinum surface: phase transition between α-PtO_2-like and β-PtO_2-like structures

Tomomi Shimazaki · Toshiya Suzuki · Momoji Kubo

Received: 16 January 2011 / Accepted: 27 July 2011 / Published online: 10 September 2011

Abstract We investigate the oxidation process of a platinum surface by using the density functional theory approach under the periodic boundary condition. This oxidation process has received much attention because it is an initial step in the dissolution of platinum catalysts in polymer electrolyte fuel cells. In this research, we determine the optimized structure of α -PtO_2-like and β-PtO_2-like oxidized platinum surfaces, which have recently been proposed on the basis of in situ X-ray diffraction analysis, at the Kohn Sham density functional theory (KS-DFT) generalized gradient approximation (GGA) level of theory. We discuss the phase transition from the α-PtO_2-like surface to the β-PtO_2-like surface, including the place-exchange reaction between oxygen and platinum atoms. We propose an intermediate structure in the phase transition, and show that the β-PtO_2-like structure can be formed directly from this intermediate structure.

Keywords Pt surface · PtO_2 surface · Oxidized surface · Quasi-3D surface · DFT · Slab model

1 Introduction

Polymer electrolyte fuel cells (PEFCs) are expected to serve as a component of clean cogeneration systems for in-vehicle and domestic use, owing to their advantageous features that include compact size, low operation temperature, and lack of greenhouse gas emission. Against this background, many experimental and theoretical studies have been carried out with the aim of developing PEFCs [1–9]. However, performance degradation of PEFCs has prevented their widespread application [10]. One cause of this degradation is the loss of the platinum catalyst's surface activity toward the cathode reaction under acidic conditions; moreover, the grain growth of platinum nanoparticles under the constant potential operation of a PEFC decreases the active area on the platinum surface [11]. The Ostwald ripening mechanism, which includes dissolution and recrystallization of platinum atoms, is the suspected mechanism of the grain growth [12, 13], and the equilibrium concentration of dissolved Pt^{2+} under acidic conditions has been experimentally observed to be a function of cell potential. Meanwhile, several thin oxidized surface formations are thought to result from applied bias potentials on the platinum surface [14]. At potentials in the range of 0.85–1.10 V, a half-monolayer of oxygen atoms is adsorbed through discharge of water molecules. At higher potentials of 1.2–1.4 V, a second half-monolayer of oxygen atoms is formed by the interfacial place-exchange reaction between oxygen atoms and surface platinum atoms. To explain this phenomenon, Jerkiewicz et al. [14] have proposed a quasi-three-dimensional model of the oxidized platinum surface, which comprises Pt^{2+} and O^{2-}. The clear relationship between the dissociation of Pt atoms and the thin oxide layer has been the target of many recent studies on the structure and growth mechanism of oxides on a platinum surface [6, 15–22]. Gu et al. [23] explored stable sites of oxygen atom adsorption on the Pt(111) surface as a function of surface coverage by using density functional theory (DFT) calculations. They discussed the stability of oxygen atoms located in the subsurface as well

Dedicated to Professor Akira Imamura on the occasion of his 77th birthday and published as part of the Imamura Festschrift Issue.

T. Shimazaki (✉) · T. Suzuki · M. Kubo
Fracture and Reliability Research Institute (FRRI), Graduate School of Engineering, Tohoku University, 6-6-11-703 Aoba, Aramaki, Aoba-ku, Sendai, Miyagi 980-8579, Japan
e-mail: t-shimazaki@rift.mech.tohoku.ac.jp

as the reaction process through which oxygen atoms diffuse into the subsurface. Although the quasi-three-dimensional structure of the oxidized platinum surface can be modeled by the formation of subsurface oxygen, understanding of the process at the atomic level remains limited. Imai et al. [24] recently proposed α-PtO_2-like and β-PtO_2-like oxidized surface models on the basis of in situ X-ray diffraction analysis, and discussed the transition between these surface structures. We present an overview of this model in Fig. 1 [24]. Figure 1a shows the Pt(111) surface. Electro-oxidation results in a PtO surface as shown in Fig. 1b. In the next step, adsorbed oxygen atoms enter into the subsurface through a place-exchange mechanism to form the α-PtO_2-like surface structure; however, the mechanism is still unclear. The α-PtO_2-like surface is formed through further oxygen adsorption. Figure 1c shows the α-PtO_2-like surface. The β-PtO_2-like surface, which has a quasi-three-dimensional structure, is accomplished by the uplift of platinum atoms and adsorption of oxygen atoms, as shown in Fig. 1d. Although Imai et al. discussed the formation of the PtO and α-PtO_2-like surfaces, this paper will focus on the α-PtO_2-like and β-PtO_2-like PtO_2 structures, and discuss the transition process between them. Theoretical and experimental studies on the formation of a PtO surface can be found in the literature [4, 25]. The other degradation process of Pt surface, where Pt ion is directly dissolved from the PtO surface instead of forming the quasi-three-dimensional platinum oxidized surface, has been also discussed, but Imai et al. [24] suggested the importance of the α- and β-PtO_2-like surfaces as a degradation reaction. The discussion on the whole degradation processes is clearly beyond our paper, thus we concentrate on the quasi-three-dimensional structures of the platinum surface.

In this paper, we employ the generalized gradient approximation (GGA) within the Kohn Sham density functional theory (KS-DFT) framework with the periodic boundary condition to describe the electronic structure of the platinum surface. In the following section, we describe the detailed calculation method and model slab surfaces employed. We report and discuss the calculation results in Sect. 3, and we present our concluding remarks in Sect. 4.

2 Calculation method

All oxidized platinum slab model surfaces in this paper, which include the α-PtO_2-like and β-PtO_2-like surfaces and the intermediate structure between them, are created from the Pt(111) surface. We employ (4×4) and (3×3) supercell slab models with three platinum layers for α-PtO_2-like and β-PtO_2-like surfaces, respectively. The Dmol [3] software package is employed for the KS-DFT calculations in this study [26, 27]. We use a double-numeric polarized basis set with a global-space cutoff of 4.5 Å and a smearing-factor of 0.005 a.u. for all calculations [26, 27]. In order to take into account the oxidized platinum surface, we adopt the periodic boundary condition using a Monkhorst–Pack grid of $3 \times 3 \times 1$. The effective core potential is used to describe the core electrons [26, 27]. The charge density is represented by the octupole multipolar expansion. We use the Perdew and Wang [28] (PW91) GGA exchange correlation (XC) functional to investigate the optimized structures and reaction paths in Sect. 3. Table 1 shows the total energy of the optimized α-PtO_2 surface structures obtained from the PW91 XC functional; details of the table will be discussed in the following section. In order to test the functional-dependency for our simulation models, we also perform calculations using the Perdew–Burke–Ernzerhof (PBE) XC functional [29], and the results are summarized in Table 1. Use of the PBE XC functional does not result in a difference in the relative energy relationship between the α-PtO_2 surface models. For example, the fcc-tetrahedral-II

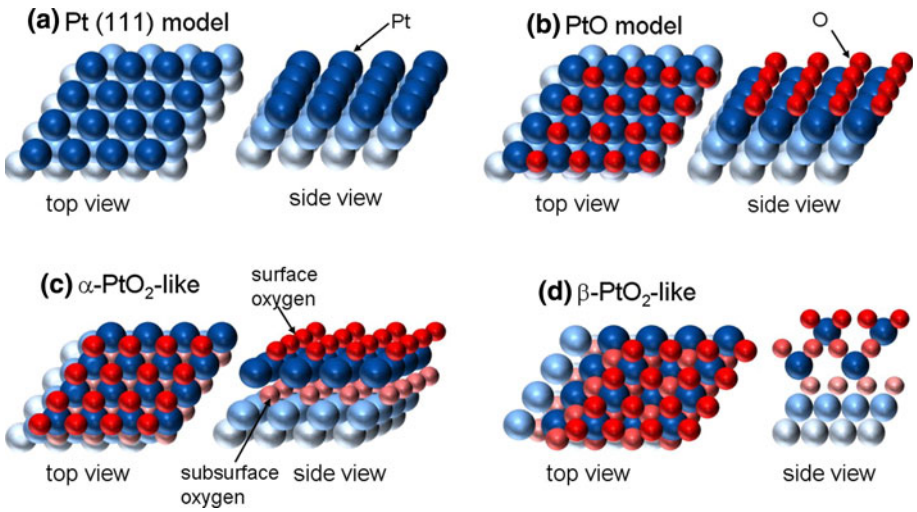

Fig. 1 Surface-oxidation process to form quasi-three-dimensional oxidized platinum surface. **a** Pt(111) model surface, **b** PtO surface model with atomic oxygen at fcc-hollow sites, **c** monolayer α-PtO_2-like surface, and **d** quasi-three-dimensional β-PtO_2-like surface

Table 1 Relative energy differences (kJ/mol) of optimized α-PtO_2-like slab surfaces from the most stable fcc-tetrahedral-II structure energy, using three platinum layers model

	PW91 energy difference (kJ/mol)	PBE energy difference (kJ/mol)
fcc-octahedral	171.2	168.5
fcc-tetrahedral-I	110.6	108.2
fcc-tetrahedral-II[a]	**0.0**	**0.0**
hcp-octahedral	21.8	20.8
hcp-tetrahedral-I	113.3	111.0
hcp-tetrahedral-II	115.0	113.3
On-top-octahedral	54.7	52.1
On-top-tetrahedral-I	85.2	82.3
On-top-tetrahedral-II	75.5	72.0

The energy values below are normalized to be the (1 × 1) size model

[a] The (1 × 1) normalized total energies of the fcc-tetrahedral-II α-PtO_2-like surface are −508.953720 and −508.674155 a.u. for the PW91 and PBE calculations, respectively

α-PtO_2-like model is the most stable surface in the both the PW91 and PBE calculations. Thus, we employ the PW91 XC functional for the calculations described in Sect. 3. For reader's conveniences, we give the information on calculation time; we execute calculations in this paper by using 3 GHz Intel-Xeon processor with 8 CPU-cores, whose computational performance is about 90 GFLOPs, and we require for about 1 or 2 weeks to obtain an optimized surface structure of the oxidized platinum surface.

3 Results and discussion

3.1 α-PtO_2-like surface structure

First, we discuss the optimized structure of the α-PtO_2-like surface based on the generalized gradient approximation exchange correlation functional; here, we employ the PW91 functional. From this calculation, we assign the position (site) of oxygen atoms as shown in Fig. 2. In this paper, oxygen atoms adsorbed on the first platinum layer are classified into three groups: (a) on-top, (b) hcp-hollow, and (c) fcc-hollow. In addition to these, (d) octahedral, (e) tetrahedral-I, and (f) tetrahedral-II sites are used to distinguish the buried oxygen atoms in the first and second platinum layers (i.e., subsurface oxygen atoms). Thus, we can determine nine different optimized α-PtO_2-like model surfaces from the surface and subsurface oxygen atoms, and the calculated total energy values are summarized in Table 1. These calculations are carried out using (4 × 4) super-cell slab surface models with three platinum layers, but the energy values presented in Table 1 are normalized to be the (1 × 1) size model. The most stable surface is the

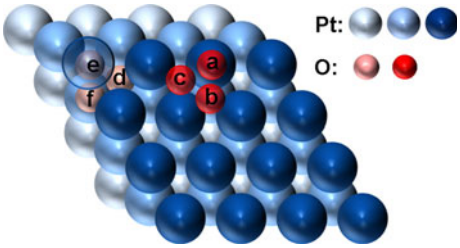

Fig. 2 Surface and subsurface oxygen atoms. **a** on-top site, **b** hcp-hollow site, **c** fcc-hollow site, **d** octahedral site, **e** tetrahedral-I site, and **f** tetrahedral-II site

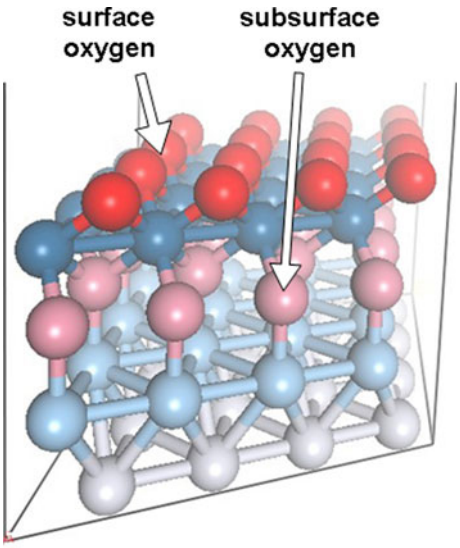

Fig. 3 Optimized fcc-tetrahedral-II α-PtO_2-like surface

fcc-tetrahedral-II model, in which the surface oxygen atoms are adsorbed onto the fcc-hollow site, and the subsurface oxygen atoms are located at the tetrahedral-II site. The fcc-tetrahedral-II model is shown in Fig. 3. In contrast, in the second most stable model, the hcp-hollow and the octahedral sites are used for the surface and subsurface oxygen atoms, respectively. Here, the (1 × 1) normalized energy difference between these α-PtO_2-like surfaces is about 20 kJ/mol. This result may suggest that atomic-scale local distortions can easily occur in the α-PtO_2-like surface.

Our preliminary KS-DFT calculations have indicated that the fcc-hollow site is the most stable one for adsorbed oxygen atoms for the PtO surface. Gu et al. [23] examined the most stable site of atomic oxygen adsorption on Pt(111) as a function of surface coverage, and they also reported that the fcc-hollow site is the most stable. These calculations suggest that the structure of the α-PtO_2-like surface is influenced by the stability of oxygen atom located on the fcc-hollow site; the surface oxygen atoms are located on the fcc-hollow site in the most stable α-PtO_2-like surface. However, the subsurface oxygen atoms introduce complexity to the energy relationship among α-PtO_2-like model

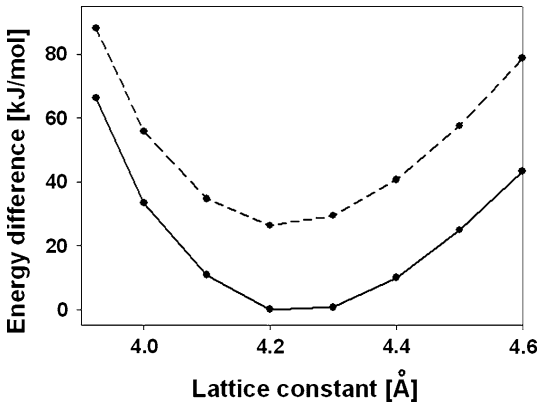

Fig. 4 Energy differences (kJ/mol) of α-PtO_2-like surface as a function of lattice constant, here the energies are normalized to be the (1 × 1) size model. *Solid line* indicates the fcc-tetrahedral-II model, and *dashed line* indicates the hcp-octahedral model. The origin of the energy is the optimized energy of the fcc-tetrahedral-II model. α-PtO_2-like surfaces are represented here by the slab model with three platinum layers

surfaces. For example, the surface oxygen atoms of the second stable model, that is, the hcp-octahedral model, are located at the hcp site rather than the fcc site, owing to the packed structure of the α-PtO_2-like models. The ion radius of O^{2-} is considerably large (about 1.4 Å), and therefore subsurface oxygen atoms tend to be located at spacious sites, and the characteristics of the location strongly affect the position of surface oxygen. In other words, steric effects plays a key role governing the structure of α-PtO_2-like surface. Imai et al. [24] reported that oxides can be easily grown at the surface of the platinum nanoparticles from the X-ray absorption spectroscopy (XAS) and the electrochemical experiment, and suggested that the surface of the platinum particles are covered with oxides, whereas the core of the metal platinum remains the fcc structure. In our calculations, the model surfaces are completely oxidized due to the theoretical periodic conditions, thus our models are suitable to reflect the experimental situation. In the calculations of the α-PtO_2-like surfaces, we use the lattice constant of bulk Pt (3.92 Å). Figure 4 shows the total energy of α-PtO_2-like model as a function of the lattice constant; here, the solid and dashed lines indicate the fcc-tetrahedral-II (most stable) and hcp-octahedral (second stable) models, respectively. The energies displayed in Fig. 4 are normalized to be the (1 × 1) size model, and the origin of the y-axis is set to be the optimization energy of the α-PtO_2-like fcc-tetrahedral-II model. To obtain the figure, we uniformly expand the α-PtO_2-like surface. Both models have the lowest total energy at a lattice constant of 4.2 Å. The Pt–Pt distance is 2.78 Å for the fcc-tetrahedral-II model with a lattice constant of 3.92 Å. However, the distance becomes larger, 2.97 Å, when the lattice constant is 4.2 Å. This calculation clearly shows that the α-PtO_2-like surface is compressed when the lattice constant is set to the value of bulk Pt (3.92 Å). This type of compression cannot be observed in the case of the PtO surface, but the α-PtO_2-like surface tends to expand the lattice. Imai et al. [24] experimentally observed the lengthening of the Pt–Pt distance during the oxidation process in the formation of the α-PtO_2-like surface, and they claim that its distance becomes 3.1 Å. The value is closer to our calculation result of 2.97 Å, which is obtained from the stable expanded α-PtO_2-like surface model. However, we should note a limitation of our ab initio calculations. In the present study, we use a slab model with three platinum layers; if we were to consider more platinum layers, the plot in Fig. 4 would be affected. The destabilization of the platinum layers would overcome the stabilization of the oxidized surface if the model were expanded. This means that the estimation of the expansion depends on the model employed. Consequently, the exact numerical estimation of the expansion is difficult within the framework of the slab model. On the other hand, the cluster model might be more suitable for investigating this problem, even though its calculation cost is high. Although the expansion (relaxation) process of the α-PtO_2-like surface is an interesting topic, we do not focus on that problem because the relaxation does not affect the relative energy relationships among the α-PtO_2-like models, as shown in Fig. 4; the fcc-tetrahedral-II model is most stable even if the models are uniformly expanded. In addition, the β-PtO_2-like surface structure has a lattice constant closer to that of the bulk platinum. Thus, in the following section, we concentrate on the slab model of the β-PtO_2-like structure with the same lattice constant as the platinum bulk.

3.2 Transition to the β-PtO_2-like surface

In this section, we discuss the phase transition from the α-PtO_2-like surface structure to the β-PtO_2-like surface structure. The driving force of this transition is the lattice constant mismatch between the α-PtO_2-like surface structure and the bulk platinum, that is, the β-PtO_2-like surface structure is formed to relax the α-PtO_2-like surface. First, we focus on the process where a platinum atom moves to the oxidized surface. Figure 5 shows the changes in energy along the reaction path. Figure 5 also has two insets: the structure ($x = 0.3$), which has the highest energy on the reaction path, and the final structure ($x = 1.0$). Here, the reaction path is obtained from the following procedure. (1) We determined the initial and final structures from optimization calculations. The final structure is shown in the right inset of Fig. 5. (2) The reaction coordinate $\mathbf{R}_x$ is defined as $\mathbf{R}_x = (1-x)\mathbf{R}_{\text{initial}} + x\mathbf{R}_{\text{final}}$, where $\mathbf{R}_{\text{initial}}$ and $\mathbf{R}_{\text{final}}$ are the coordinates of all atoms of the initial and final structures, respectively. Note, however, that only the

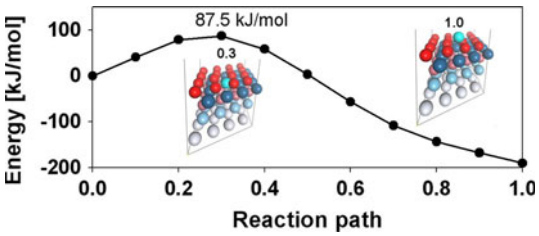

Fig. 5 Reaction energy of process of Pt atom uplift to the oxidized surface. *Insets* show the structure ($x = 0.3$) and final structure ($x = 1.0$)

surface oxygen atoms are structurally optimized and relaxed through the constrained optimization calculation. Thus, we can take into account the relaxation process of surface atoms on the reaction path. If we do not consider the surface relaxation, the reaction barriers calculated becomes much higher. In the structure ($x = 0.3$), we can observe that surface oxygen atoms around the uplifted Pt atom are moved aside by the relaxation. Conversely, the surface Pt atoms are fixed in our calculations because their steric effects on the reaction are lower than those of the surface oxygen atoms, but we should note that our calculation result yields an upper limit for the reaction barrier. The total energy of the final structure is lower than the initial structure because of the relaxation of the packed α-PtO_2-like structure. The stabilized energy is -190.3 kJ/mol. The reaction barrier is 87.5 kJ/mol. Thus, we can confirm that the reaction can proceed.

Next, we consider which platinum atom can be easily lifted up to the oxidized surface when a Pt atom is already located in the top layer. Figure 6a shows three possible reaction processes for the subsequent platinum atom displacement to the oxidized surface. In this paper, the movement (uplift) of the platinum atom A is referred as reaction process A, and the reaction processes B and C are similarly defined for platinum atoms B and C, respectively. Here, the vacancy in Fig. 6a is introduced from the initially uplifted Pt atom. Figure 6b and c present the structure ($x = 0.3$) and the final structure ($x = 1.0$) of reaction process A, respectively. Figure 7 shows the calculation results for reaction process A; here, we determined the reaction coordinates in the same manner used to obtain the results shown in Fig. 5. The stabilized energy and the reaction barrier are -136.1 and 89.9 kJ/mol, respectively. This calculation result suggests that reaction process A can proceed after a Pt atom initially moves to the oxidized surface. On the other hand, other reaction processes cannot occur because of high reaction barriers, the values of which are 177.7 and 115.0 kJ/mol for reactions B and C, respectively, even though both final structures are stabilized. The stabilization energies are -170.9 and -109.7 kJ/mol for reaction processes B and C, respectively. From these calculations, we can predict the intermediate structure in the transition to the β-PtO_2-like surface structure in Fig. 8a, where the structure is formed through reaction process A. To obtain the structure, we employ a (3×3) super-cell slab model. The (1×1) normalized total energy of the intermediate model is -508.970 a.u. The (1×1) normalized total energy of the fcc-tetrahedral-II structure is -508.954 a.u.; therefore, we can confirm that the intermediate structure of Fig. 8a is more stable. The formation of the intermediate structure should require a reaction time of the order of minutes or seconds, owing to the high energy barrier of the place-exchange reaction discussed in Figs. 5 and 7. Imai et al. [24] experimentally observed that several tens to hundreds of seconds could be necessary to achieve the transition, in support of our calculation result. The β-PtO_2-like surface structure can be formed by the further oxidization process via the intermediate structure. We discuss the structure of the β-PtO_2-like surface in the following section.

3.3 β-PtO_2-like surface structure

We show the optimized β-PtO_2-like surface structure in Fig. 8b; this structure is directly obtained from the intermediate structure shown in Fig. 8a through the adsorption of oxygen atoms on the top layer. Here, the structure is represented as a (3×3) super-cell slab model with three platinum layers. The oxygen atoms of the top oxidized layer lie directly on the third oxidized layer. The (1×1) normalized total energy is -584.133 a.u.. The Pt–Pt and Pt–O bond lengths of the β-PtO_2-like surface are summarized in Table 2. In the experimental analysis of the extended X-ray absorption fine structure (EXAFS) spectroscopy, the longer Pt–Pt bond length of about 3.5 Å is observed during the oxidization process of the surface of the platinum nanoparticles [24]. This value is close to the second nearest-neighbor (NN) Pt–Pt bond length of the β-PtO_2-like surface structure obtained from our DFT calculation. Table 2 also summarizes other bond lengths for not only the β-PtO_2-like surface but also the α-PtO_2-like and intermediate structures. We should note that the adsorption of the top oxygen atoms on the β-PtO_2-like surface only slightly disturbs the underlying structure. To confirm the stability of the β-PtO_2 surface structure shown in Fig. 8b, we calculate another β-PtO_2-like structure, which is obtained from the hcp-octahedral α-PtO_2-like model. The β-PtO_2-like structure gives -584.110 a.u. for the (1×1) normalized total energy. We summarize these calculation results in Table 3. From these calculations and the formation process discussed in the previous section, we can conclude that the β-PtO_2-like surface structure shown in Fig. 8b is the most stable.

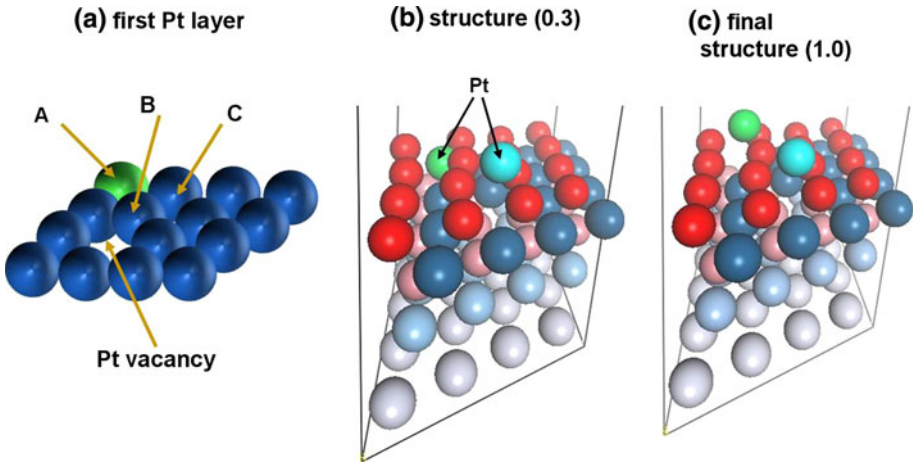

Fig. 6 **a** Three possible sequential reaction processes after a Pt atom, where the vacancy represents the site, is moved up to the *top* layer. In reaction *A*, platinum atom A is lifted up to the oxidized surface. Similar definitions can be used for reaction processes *B* and *C*. **b** The structure ($x = 0.3$) and **c** the final structure ($x = 1.0$) of reaction *A*

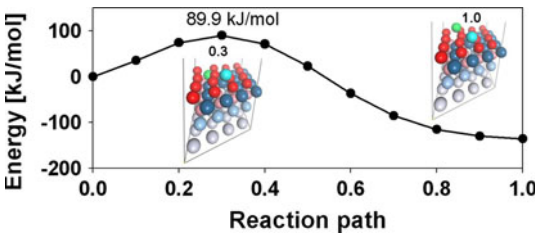

Fig. 7 Energy changes along reaction process A. *Insets* show the structure ($x = 0.3$) and the final structure ($x = 1.0$)

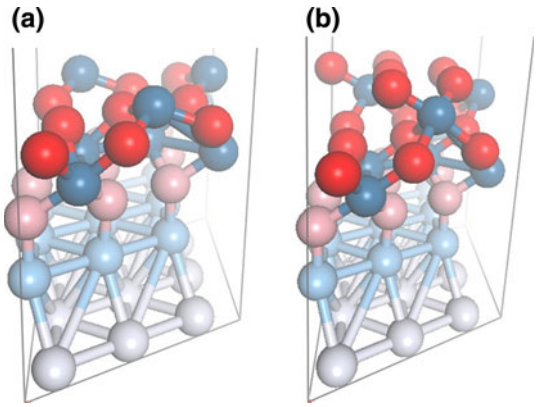

Fig. 8 **a** Optimized intermediate structure between α-PtO_2-like and β-PtO_2-like surfaces. **b** Optimized structure of β-PtO_2-like surface formed from the fcc-tetrahedral-II α-PtO_2-like surface through further adsorption of atomic oxygen

4 Concluding remarks

In this paper, we discussed the optimized structure of α-PtO_2-like and β-PtO_2-like surfaces on the basis of KS-DFT calculations. In addition, we discussed the transition process between these structures. The KS-DFT calculation revealed that the fcc-tetrahedral-II model is most stable for the α-PtO_2-like surface, and the most stabilized β-PtO_2-like structure is directly formed from this surface structure. In this paper, we also present the intermediate

Table 2 Pt–Pt and Pt–O bond lengths (Å)

	First NN Pt–Pt	Second NN Pt–Pt	First NN Pt–O	Second NN Pt–O
α-PtO_2	2.775		2.044	
Intermediate structure (Fig. 8a)	2.775	3.603	2.029	2.031
β-PtO_2	2.775	3.604	2	2.02

Table 3 Relative energy difference (kJ/mol) of β-PtO_2-like oxidized structure, using three platinum layers model

	Energy difference (kJ/mol)
β-PtO_2 surface formed from fcc-tetrahedral-II α-PtO_2 model[a]	**0.0**
β-PtO_2 surface formed from hcp-octahedral α-PtO_2 model	60.5

The energy values below are normalized to be the (1×1) size model

[a] The (1×1) normalized total energy of the model is −588.132999 a.u.

structure of the transition process between α-PtO_2-like and β-PtO_2-like surfaces by considering the energy changes in place-exchange reactions of a platinum atom. The energy barriers of those elementary steps were about 90 kJ/mol; therefore the elementary place-exchange oxidation process is found to be possible in an actual oxidation reaction.

This paper focused on the formation of the β-PtO_2-like surface structure. A remaining problem is the formation of the α-PtO_2-like local structure from the PtO surface; however, the transition process may be more complex because an amorphous structure has been experimentally observed during the formation of the α-PtO_2-like local structure [24]. We show the close normalized energy difference between the most stable fcc-tetrahedral-II structure

and the second stable hcp-octahedral structure for the α-PtO_2-like surface in Table 1. The amorphous structure may include local distortions such as the hcp-octahedral structure due to the close energy difference. Moreover, from experiments, the surface platinum metal is reported to be relaxed as a result of the large lattice mismatch between the α-PtO_2-like layer and platinum metal [24]. This structural relaxation process may play a critical role in the formation of the α-PtO_2-like local structure. Our preliminary calculations rule out the direct penetration of an oxygen atom into the Pt core metal. The uplift place-exchange process of Pt atom might occur in the first stage of the formation of the α-PtO_2-like structure. The PtO surface and the penetration process of oxygen atom is discussed in the other literatures, and those kinds of studies may be useful to reveal the complicated formation process of the α-PtO_2-like local structure [6, 20–23].

We do not consider the effects of water solvent [30], acidic environment [31], and cations and anions [32]. Although these effects warrant careful investigation, our findings may not be largely influenced by these effects because the optimized structure of the α-PtO_2-like and β-PtO_2-like surfaces are, to a large extent, governed by steric effects due to the large atomic radius of oxygen. In other words, the stable structure is primarily related to the packing of platinum and oxygen atoms. Thus, other factors might only slightly perturb the optimized structure. These perturbative behaviors of cations, anions, and acids may be experimentally proven if only small changes are observed in the in situ X-ray experiments with their different concentrations. However, we should comment that those can affect the energetic aspects, for example the water solvent with ions and acidic environment may change the reaction barriers discussed in this paper, and those effects are important for other chemical systems [22, 33, 34]. On the other hand, we may need to pay attention to the potential voltage effect on the platinum metal surface because its influence is not still understood well within the framework of first-principles calculations. Otani et al. [35] has recently proposed the effective screening medium (ESM) method to take into account the potential voltage effect in first-principles calculations, and applied the approach to a hydrogen evolution reaction and its dynamics on the platinum surface [36]. However, such first-principles studies are still in the preliminary stage, and the consideration of the effect is beyond the aim of this paper. Many efforts to develop the Gaussian-basis-set-based ab initio calculation methods under the periodic boundary conditions have been examined [37–45], and we hope that those kinds of studies will be helpful to resolve the degradation mechanism of the platinum surface.

References

1. Savinova DV, Molodkina EB, Danilov AI, Polukarov YM (2004) Russ J Electrochem 40:683
2. Nørskov JK, Rossmeisl J, Logadottir A, Lindqvist L, Kitchin JR, Bligaard T, Jónsson H (2004) J Phys Chem B 108:17886
3. Shubina TE, Harting C, Koper MTM (2004) Phys Chem Chem Phys 6:4215
4. Teliska M, O'Grady WE, Ramaker DE (2005) J Phys Chem B 109:8076
5. Roth C, Benker N, Buhrmester T, Mazurek M, Loster M, Fuess H, Koningsberger DC, Ramaker DE (2005) J Am Chem Soc 127:14607
6. Walch S, Dhanda A, Aryanpour M, Pitsch H (2008) J Phys Chem C 112:8464
7. Ma Y, Balbuena PB (2008) J Phys Chem C 112:14520
8. Choe Y-K, Tsuchida E, Ikeshoji T, Yamakawa S, Hyodo S (2008) J Phys Chem B 112:11586
9. Choe Y-K, Tsuchida E, Ikeshoji T, Yamakawa S, Hyodo S (2009) Phys Chem Chem Phys 11:3892
10. Borup R, Meyers J, Pivovar B, Kim YS, Mukundan R, Garland N, Myers D, Wilson M, Garzon F, Wood D, Zelenay P, More K, Stoh K, Zawodzinski T, Boncella J, McGrath JE, Inaba M, Miyatake K, Hori M, Ota K, Ogumi Z, Miyata S, Nishikata A, Siroma Z, Uchimoto Y, Yasuda K, Kimijima K, Iwashita N (2007) Chem Rev 107:3904
11. Xie J, Wood-III DL, Wayne DM, Zawodzinski TA, Atanassov P, Borup RL (2005) J Electrochem Soc 152:A104
12. Ferreira PJ, Ia-O' GJ, Shao-Horn Y, Morgan D, Makharia R, Kocha S, Gasteiger HA (2005) J Electrochem Soc 152:A2256
13. Yasuda K, Taniguchi A, Akita T, Ioroi T, Siroma Z (2006) Phys Chem Chem Phys 8:746
14. Jerkiewicz G, Vatankhah G, Lessard J, Soriaga MP, Park Y (2004) Electrochim Acta 49:1451
15. You H, Zurawski DJ, Nagy Z, Yonco RM (1994) J Chem Phys 100:4699
16. Nagy Z, You H (2002) Electrochim Acta 47:3037
17. Darling RM, Meyers JP (2003) J Electrochem Soc 150:A1523
18. Alsabet M, Grden M, Jerkiewicz G (2006) J Electroanal Chem 589:120
19. Gu Z, Balbuena PB (2006) J Phys Chem A 110:9783
20. Gu Z, Balbuena PB (2007) J Phys Chem C 111:17388
21. Gu Z, Balbuena PB (2008) J Phys Chem C 112:5057
22. Roudgar A, Eikerling M, van-Santen R (2010) Phys Chem Chem Phys 12:614
23. Gu Z, Balbuena PB (2007) J Phys Chem C 111:9877
24. Imai H, Izumi K, Matsumoto M, Kubo Y, Kato K, Imai Y (2009) J Am Chem Soc 131:6293
25. Tian F, Anderson AB (2008) J Phys Chem C 112:18566
26. Delley B (1990) J Chem Phys 92:508
27. Delley B (2000) J Chem Phys 113:7756
28. Perdew JP, Chevary JA, Vosko SH, Jackson KA, Pederson MR, Singh DJ, Fiolhais C (1992) Phys Rev B 46:6671
29. Perdew JP, Burke K, Ernzerhof M (1996) Phys Rev Lett 77:3865
30. Hamada I, Morikawa Y (2008) J Phys Chem C 112:10889
31. Mitsushima S, Koizumi Y, Uzuka S, Ota K (2008) Electrochim Acta 54:455
32. Yadav AP, Nishikata A, Tsuru T (2007) Electrochim Acta 52:7444
33. Suzuki K, Kuroiwa Y, Takami S, Kubo M, Miyamoto A, Imamura A (2002) Solid State Ion 152–153:273
34. Jalkanen KJ, Degtyarenko IM, Nieminen RM, Cao X, Nafie LA, Zhu F, Barron LD (2008) Theor Chem Acc 119:191
35. Otani M, Sugino O (2006) Phys Rev B 73:115407

36. Otani M, Hamada I, Sugino O, Morikawa Y, Okamoto Y, Ikeshoji T (2008) Phys Chem Chem Phys 10:3609
37. Shimazaki T, Asai Y (2008) Chem Phys Lett 466:91
38. Shimazaki T, Asai Y (2009) J Chem Theory Comput 5:136
39. Shimazaki T, Asai Y (2009) J Chem Phys 130:164702
40. Shimazaki T, Hirata S (2009) Int J Quantum Chem 109:2953
41. Hirata S, Shimazaki T (2009) Phys Rev B 80:085118
42. Hirata S, Sode O, Keceli M, Shimazaki T (2010) In: Manby FR (ed) Accurate condensed-phase quantum chemistry. CRC Press, Boca Raton, p 129
43. Shimazaki T, Asai Y (2010) J Chem Phys 132:224105
44. Shimazaki T, Kubo M (2011) Chem Phys Lett 503:316
45. Shimazaki T, Asai Y (2011) Gaussian and forueir transform (GFT) method and screened Hartree-Fock exchange potential for first-principles band structure calculations. In: Nikolic GS (ed) Fourier transform—approach to scientific principles. Rijeka, Intech